Geol. Mag. **148** (*5–6*), *2011, pp. 802–818. © Cambridge University Press 2011*
doi:10.1017/S0016756811000422

Cr-spinel compositions in serpentinites and their implications for the petrotectonic history of the Zagros Suture Zone, Kurdistan Region, Iraq

KHALID J. A. ASWAD*, NABAZ R. H. AZIZ‡ & HEMIN A. KOYI§†

*Department of Geology, College of Science, Mosul University, Iraq
‡Department of Geology, College of Science, Sulaimani University, Kurdistan Region, Iraq
§Department of Earth Sciences, Uppsala University, Uppsala, Sweden

(*Received* 23 August 2010; *accepted* 22 March 2011)

Abstract – Accessory chrome spinels are scattered throughout the serpentinite masses in two allochthonous thrust sheets belonging to the Penjween–Walash sub-zone of the northwestern Zagros Suture Zone in Kurdistan. Based on field evidence, the serpentinites are divided into two groups: (1) highly sheared serpentinites (110–80 Ma), which occupy the lower contact of the ophiolitic massifs of the Upper Allochthonous sheet (Albian–Cenomanian age), and (2) ophiolitic mélange serpentinites of mixed ages (150 and 200 Ma) occurring along thrust faults on the base of the volcano-sedimentary segment (42–32 Ma) of the Lower Allochthonous sheet. The Cr-spinels of both groups show a wide range of Y_{Cr} (Cr/(Cr + Al) atomic ratio) from 0.37 to 1.0, while the X_{Mg} (Mg/(Mg + Fe^{2+}) atomic ratio) ranges from 0.0 to 0.75. Based on the Cr-spinel compositions of the entire dataset and in conjunction with back-scattered electron imaging, from core to rim, three spinel stages have been recognized: the residual mantle stage, a Cr-rich stage and a third stage showing a very narrow magnetite rim. These three stages are represented by primary Cr-spinel, pre-serpentinization metamorphosed spinel and syn- or post-serpentinization spinel, respectively. The chemical characteristics of primary (first-stage) Cr-spinels of both serpentinite groups indicate a tectonic affinity within a fore-arc setting of peridotite protoliths. The second stage indicates that Cr-spinels have undergone subsolidus re-equilibration as a result of solid–solid reaction during pre-serpentinization cooling of the host rock. Here the primary Cr-spinel compositions have been partly or completely obscured by metamorphism. During the third stage, the Cr-spinels have undergone solid–fluid re-equilibration during syn- or post-serpentinization processes. Both the second and third stages point to diachronous metamorphic paths resulting from continuous tectonic evolution influenced by either slow or fast uplift of mantle protoliths. In the fast metamorphic paths, the primary chrome spinels are flanked by a very narrow magnetite rim. The presence of two groups of distally separated serpentinites with different emplacement ages and fore-arc tectonic affinity could indicate that the closure of the Tethys Ocean culminated in two fortuitous subduction processes.

Keywords: serpentinite, Zagros, Cr-spinel, Kurdistan Region, tectonic.

1. Introduction

Suture zones on many continents represent significant collisional tectonic boundaries between terranes of different affinities, and reflect continental growth. However, despite their tectonic significance and the complexity of the processes that form them, they are poorly understood. Serpentinites, which are highly lubricating and easily weathered, are key elements in understanding subduction and exhumation processes and have played an important role in the tectonics of the Zagros Suture Zone (Buday & Jassim, 1987). This is more evidenced in Paleocene–Eocene units, where terrigenous sediments derived mainly from the serpentinite mélange (Dhannoun, Al-Dabbagh & Hasso, 1988) dominate the eastern side of the Tertiary molasse basins. Chrome spinel is of particular significance to serpentinite provenance studies for a variety of reasons: (1) spinels either derive from different degrees of partial melting of upper-mantle peridotite or crystallize from mafic and ultramafic magmas over a wide range of conditions. They are therefore sensitive indicators of the original host rock composition (Irvine 1967; Allan, Sack & Batiza, 1988; Roeder, 1994). (2) The unusual chemical durability of Cr-spinel makes its original composition more likely to be preserved against processes of pre- and syn-serpentinization, implying that the petrogenetic discrimination fields of Cr-spinel apply to the provenance of serpentinites as well as to their tectonogenetic affinity (e.g. Pober & Faupl, 1988; Cookenboo, Bustin & Wilks, 1997). Owing to an increasing economic interest, the geochemistry and tectonogenesis of Tethyan nodular chromites have received much attention during the last few decades (Moghadam, Rahgoshay & Forouzesh, 2009) compared to disseminated Cr-spinels in serpentinite bodies. In contrast, the present study exclusively deals with Cr-spinel compositions in eight distally separated serpentinite bodies associated with the Upper Allochthon (Albian–Cenomanian) and Lower

†Author for correspondence: Hemin.Koyi@geo.uu.se

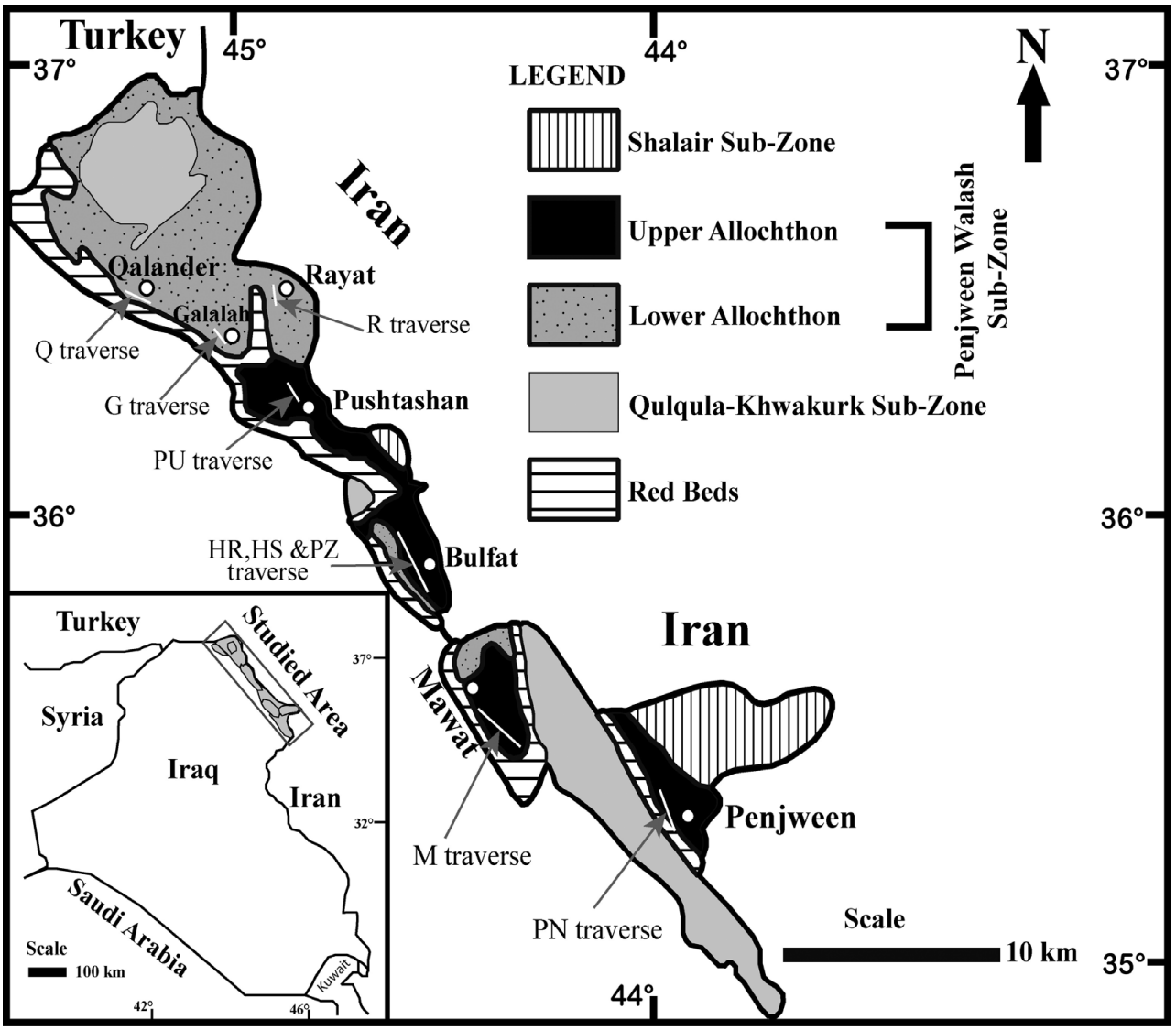

Figure 1. Geological map of the study area showing the location of sample traverses.

Allochthon (Palaeogene) within the Penjween–Walash sub-zone in an attempt to fingerprint the serpentinite sources of the Zagros ophiolites and to reconstruct the tectonic setting of the northwestern Zagros Suture Zone in the Kurdistan Region.

2. Geological overview

The northwestern Zagros Suture Zone is located in the Kurdistan Region (Iraq) and is part of the Zagros fold–thrust belt (Koyi, 1988) (Fig. 1). The zone occupies an area of about 5000 km^2 along the Iraq–Iran–Turkey borders and comprises three tectonic (sub-) zones. From the outer part of the suture zone inwards, these are the Qulqula–Kwakurk, Penjween–Walash and Shalair sub-zones (Jassim & Buday, 2006). The Penjween–Walash sub-zone exhibits several serpentinite bodies within two allochthonous thrust sheets (N. Aziz, unpub. Ph.D. thesis, Sulaimani Univ., Iraq, 2008). Based on field evidence, there are two types of serpentinite bodies: the first is the ophiolite suite serpentinites (ophiolite–serpentinite associates), connected with the Upper Cretaceous ophiolitic massifs (Upper Allochthon) of Penjween, Mawat, Bulfat and Pushtashan. The second type is the serpentinite imbricates (ophiolitic mélange serpentinites), occurring mostly along thrust faults that juxtapose the Qulqula Radiolarite with the overlying Tertiary volcano-sedimentary segment of the Walash–Naopurdan allochthonous thrust sheet (Lower Allochthon) (N. Aziz, unpub. Ph.D. thesis, Sulaimani Univ., Iraq, 2008). The radiometric ages of the studied serpentinites, obtained with Rb–Sr methods, range between 80 and 110 Ma for ophiolite–serpentinite associates (Aziz, Elias & Aswad, 2011). This age is consistent with that of the Mawat ophiolite of Albian–Cenomanian age (118–97 Ma) (Aswad & Elias, 1988; Aswad, 1999). The serpentinite imbricates, however, contain sporadic exotic blocks of metabasalts and metasediments which are tectonically intermingled with the serpentinite-hosted matrix, forming a serpentinite mélange. The latter represents a complex mixture of various rocks consistent with a mainly ophiolitic origin (Aziz, Aswad & Koyi, 2011, this issue). The mixed ages of this ophiolitic mélange

https://doi.org/10.1017/S0016756811000422 Published online by Cambridge University Press

serpentinite, obtained by Rb–Sr methods, however, range from 150 to 200 Ma in comparison with the overlying Lower Allochthon (43–32 Ma; A. Koyi, unpub. M.Sc. thesis, Mosul Univ., Iraq, 2006). In practice this age range is of little use other than indicating that the ophiolitic mélange serpentinite is older than the Mawat ophiolites. The ophiolitic massifs have almost all the characteristic members of an ophiolite suite, and the highly sheared basal serpentinites (110–80 Ma) are juxtaposed onto island arc volcanites (Walash volcano-sedimentary sequence) (42–32 Ma). Accordingly, the ophiolite massifs were thrust over the island arc volcanic rocks in late Palaeogene or early Neogene time. However, when the serpentinite mélange was emplaced is very uncertain owing to the lack of accurate dating of syntectonic flysch and molasse deposits, and the emplacement is more likely to have taken place before the resorption of the oceanic lithosphere. The emplacement of the serpentinite mélange may be synchronous with late flysch sedimentation of Tanjero (Maastrichtian). Field observations concerning the upper part of the Tanjero flysch deposits suggest that the serpentinite-derived terrigenous sediments are of ophiolitic origin. These sediments are either derived from the advancing ophiolite nappes (Karim *et al*. 2009) or from ophiolitic mélange serpentinites. However, this study suggests that the ophiolitic mélange serpentinites are the more likely source of the Tanjero flysch deposits. This is because the Neo-Tethyan strand remained open in front of advancing ophiolite nappes, separating the latter from the mentioned accretionary complex terrane–foreland basin assemblages.

3. Analytical techniques

The chemical compositions of Cr-spinel in the serpentinites were determined by an electron microprobe technique at the Department of Geology, University of Uppsala, Sweden, using an AMECA SX50 microprobe. The operating conditions were 20 kV accelerating potential and 15 nA beam current; probe size, normally 1–2 micrometres. Quality control was maintained by analysing a standard Cr_2O_3 (Cr), Fe_2O_3 (Fe), NiO (Ni) sample during each electron microprobe session. The proportion of Fe^{2+} and Fe^{3+} in spinel was calculated by assuming spinel stoichiometry.

4. Petrography and mineral chemistry

4.a. Petrography

The mineral assemblages of the Zagros Suture Zone serpentinites were determined by petrography and XRD techniques. These mineralogical assemblages indicate that the original ultramafic protoliths are harzburgite, dunite and to a small extent lherzolite, which were serpentinized under greenschist to amphibolite-facies conditions. The serpentinite comprises variable proportions of predominantly a serpentine polymorph (most common are lizardite and chrysotile with minor amounts of antigorite, which is restricted to sheared-type serpentinite of the Penjween and Galalah serpentinite), along with olivine, pyroxene, spinel, amphibole, chlorite, talc and carbonates. Relict olivine occurs as porphyroblasts in partly serpentinized samples, while in mylonitized serpentinite of the Penjween area, it occurs as elongate grains. As serpentinization proceeded, olivine was replaced by formation of lizardite, and then lizardite itself might have been replaced by chrysotile. In the completely serpentinized peridotites, the altered orthopyroxenes (bastites) retain their original shape; relict orthopyroxenes occur as elongate porphyroclasts or as aggregates of deformed crystals and they retain the altered exsolution lamellae. Clinopyroxene usually occurs as porphyroclasts or a subhedral crystal in serpentinites whose protolith is lherzolite. Magnetite in Zagros Suture Zone serpentinites is predominantly secondary, and it is a by-product of chromite alteration and alteration of olivine and orthopyroxene. The most commonly preserved textures of the studied serpentinites are of a pseudomorphic type (mesh, bastite and hourglass) after olivine and pyroxene, which preserve the pre-serpentinization textures of the ultramafic precursor, as well as non-pseudomorphic (interpenetrating and interlocking) textures. The sheared type of serpentinite is characterized by an interpenetrating (tiger-skin) texture (Aziz, Aswad & Koyi, 2011). Accessory chrome spinel is scattered throughout the serpentinite masses, and occurs as disseminated anhedral to subhedral crystals and/or irregular grains. Most of these grains are brecciated, fractured and altered along fractures and grain boundaries (Fig. 2a). The pre-existing spinel grains are rimmed or mantled by magnetite owing to alteration processes, with numerous intersects filled with serpentine minerals (Fig. 2b). They are also irregularly distributed in the matrix, away from the spinel rims and in the serpentine interstices, forming fine opaque material stringers during serpentinization. Magnetite, which can easily be recognized in back-scattered electron (BSE) imaging (Cookenboo, Bustin & Wilks, 1997), occupies the outermost rim around Cr-spinel. The Cr_2O_3 content of magnetite ranges from 0 to 1.52 % and for Cr-magnetite is $\sim$ 25 % (N. Aziz, unpub. Ph.D. thesis, Sulaimani Univ. Iraq, 2008). BSE imaging is employed to distinguish different zones of spinel by using the contrast function, which essentially depends upon differences in average atomic number (AN) of the zones. The location chosen for an electron-microprobe analysis is usually guided by differences in BSE images.

In extensively serpentinized samples from all the studied serpentinite bodies, primary Cr-spinel has been metamorphosed and/or altered into ferritchromite at higher temperatures or into Cr-bearing magnetite at lower temperatures (Lee, 1999; Ahmed, Arai & Attia, 2001). Based on the contrast in BSE imaging, metamorphosed Cr-spinels exhibit either continuous

https://doi.org/10.1017/S0016756811000422 Published online by Cambridge University Press

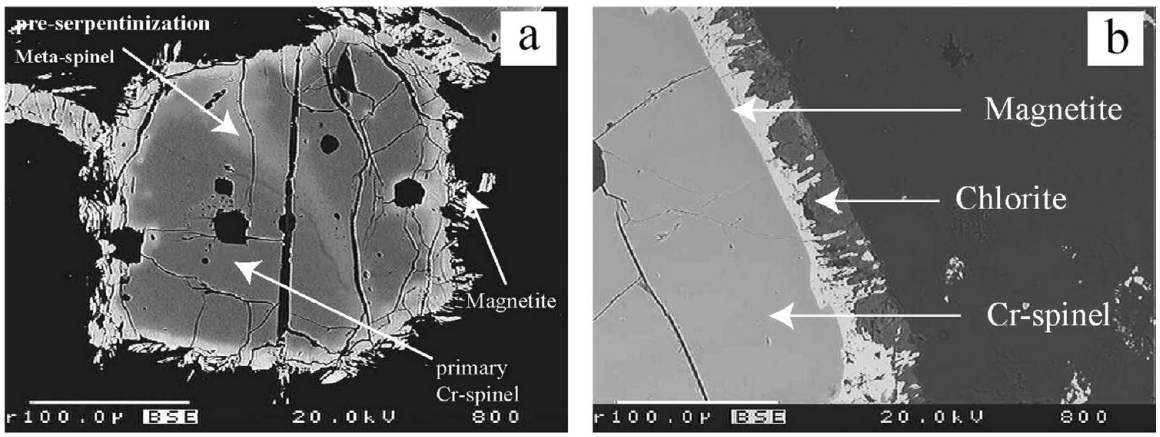

Figure 2. Back-scattered electron image of (a) Cr-spinel irregular grain which is brecciated, fractured and altered along fractures and boundaries; (b) Cr-spinel rimmed by magnetite.

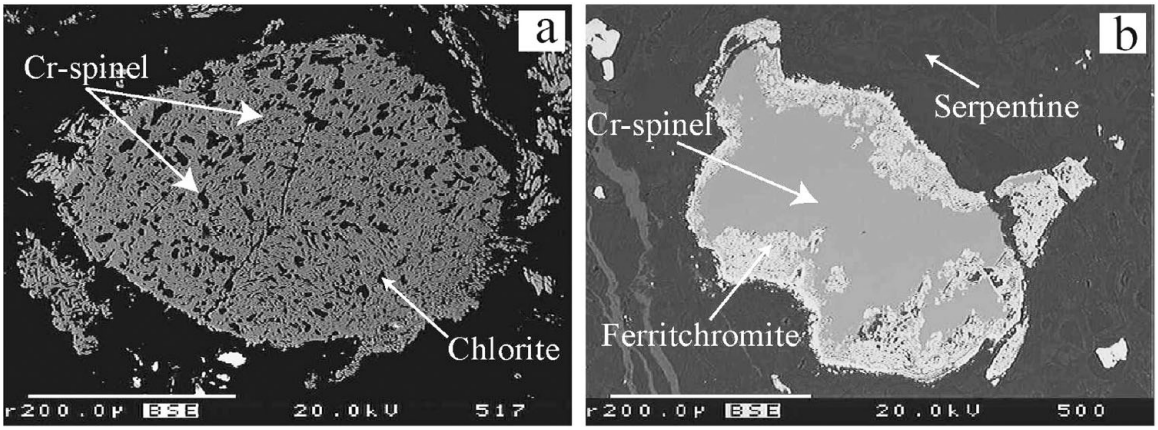

Figure 3. Cr-spinel exhibiting a spongy texture (a) and primary spinel having spongy rims with neighbouring serpentine (b).

and/or discontinuous compositional variations (i.e. from core to rim, primary Cr-spinel, ferritchromite and Cr-bearing magnetite, respectively). Although much of the Cr-spinels were metamorphosed, primary Cr-spinel grains are distinguished by the corroded primary phase mantled by ferritchromite and magnetite due to replacement processes. Detailed petrography and BSE imaging of the Cr-spinels specify mainly four different textures:

(1) A spongy texture in which a symplectite lobe around spinel porphyroclasts is composed of chlorite and vermicular Cr-rich spinel (ferritchromite) (Fig. 3a) and pyroxene–spinel symplectite probably formed by a breakdown of garnet (Takahashi & Arai, 1989). This is followed by metamorphic alteration (i.e. chloritization of pyroxene). The Cr-spinels vary from having distinct contacts with neighbouring serpentinite to having spongy rims (Fig. 3b).

(2) A protogranular texture, with linear to curvilinear grain boundaries. Grain size is up to 5 mm while a weak lineation overprints some protogranular samples (Fig. 4).

(3) A heteradcumulate texture: the intercumulus phase shows a heteradcumulus texture which partly or completely envelopes the primocryts (i.e. serpentinized olivine) (Fig. 5a).

(4) An amoeboidal texture: the magnetite rims grow irregularly away from the Cr-spinel rims and join the magnetite stringers of the serpentine matrix (Fig. 5b). The amoeboidal texture shows the retention of the original lobate morphology by the Cr-spinel core.

4.b. Cr-spinel chemistry

The chemistry of the Cr-spinel (Table 1) is expressed by the XY_2O_4 formula: divalent site X = (Fe^{2+}, Ni, Mn, Co, Zn) and trivalent site Y = (Cr^{3+}, Fe^{3+}, Al). Ti is assumed to be present as ulvo-spinel components. Iron is subdivided into ferrous and ferric to satisfy the condition Y = 2X. Plots of Cr^{3+} versus Al^{3+} and of Mg^{2+} versus Fe^{2+} for the entire dataset of Cr-spinels (Fig. 6) show clearly a 1:1 replacement of $MgAl_2O_4$ by $Fe(Cr, Fe^{3+})_2O_4$. Projection of the Cr-spinel compositions of the entire dataset onto the Fe_3O_4–$FeCr_2O_4$–$Mg_{0.65}Fe_{0.35}Al_2O_4$ plane (within the oxidized spinel prism; Fig. 7) illustrates two chemical trends of Cr-spinel. The Cr-spinel compositions investigated with BSE imaging make it more feasible

https://doi.org/10.1017/S0016756811000422 Published online by Cambridge University Press

Table 1. Chemical composition of chrome spinel in Zagros Suture Zone serpentinites, determined based on 4 oxygen atoms

% Oxides	G8-1	G8-2	G9A-3	G10A-3	G10A-4	G10A-5	G10A-6	M8A-1	M8A-1b	M8A-2	M8A-3	M8-A-4	P4-1
SiO_2	0.000	0.011	0.014	0.000	2.572	0.027	2.759	0.036	0.038	0.043	0.075	0.043	0.025
Al_2O_3	18.433	17.853	24.624	32.621	3.302	33.337	2.937	3.339	3.354	5.329	0.546	0.000	10.122
TiO_2	0.074	0.056	0.365	0.026	0.241	0.051	0.176	1.293	1.300	0.745	0.964	0.213	0.144
FeO	19.577	20.076	25.526	16.487	46.205	16.218	46.608	66.034	63.508	48.795	75.195	89.128	28.995
MnO	0.000	0.245	0.197	0.147	8.127	0.149	7.358	0.208	0.281	0.318	0.560	0.000	0.229
MgO	11.944	11.561	9.637	15.225	4.218	15.327	4.392	2.791	3.109	4.267	0.702	0.000	6.256
CaO	0.000	0.008	0.003	0.000	0.000	0.010	0.132	0.000	0.000	0.009	0.042	0.041	0.000
Na_2O	0.000	0.000	0.000	0.000	0.000	0.000	0.000	0.189	0.000	0.000	0.000	0.221	0.037
K_2O	0.000	0.002	0.000	0.000	0.000	0.000	0.000	0.000	0.000	0.000	0.000	0.000	0.000
NiO	0.069	0.000	0.000	0.188	0.360	0.130	0.338	0.263	0.265	0.088	0.198	0.033	0.025
Cr_2O_3	49.049	50.021	35.751	35.372	29.528	33.225	28.801	21.675	22.804	38.303	17.566	1.522	52.636
PROBE Σ	100.046	99.833	96.131	100.073	94.68	98.476	93.502	95.829	94.659	97.897	95.846	91.202	98.538
Fe^{3+}	5.44	5.58	7.10	4.58	12.84	4.51	12.96	18.36	17.65	13.56	20.90	24.78	16.44
Fe^{2+}	14.68	15.06	19.14	12.37	34.65	12.16	34.96	49.53	47.63	36.60	56.40	66.85	14.21
$\%Fe^{3+}$	0.25	0.25	0.25	0.25	0.25	0.25	0.25	0.25	0.25	0.25	0.25	0.25	0.51
Total	99.69	100.40	96.83	100.53	95.85	98.93	94.81	97.68	96.44	99.26	97.95	93.70	100.12
Si	0.00	0.00	0.00	0.00	0.10	0.00	0.11	0.00	0.00	0.00	0.00	0.00	0.00
Al	0.68	0.66	0.93	1.11	0.15	1.15	0.14	0.16	0.16	0.23	0.03	0.00	0.40
Ti	0.00	0.00	0.01	0.00	0.01	0.00	0.01	0.04	0.04	0.02	0.03	0.01	0.00
Cr	1.22	1.24	0.90	0.81	0.90	0.77	0.89	0.68	0.72	1.11	0.58	0.06	1.38
Fe^{3+}	0.13	0.13	0.17	0.10	0.37	0.10	0.38	0.55	0.53	0.38	0.66	0.86	0.41
Sum^{3+}	2.03	2.04	2.01	2.02	1.54	2.02	1.52	1.43	1.45	1.74	1.30	0.93	2.19
Fe^{2+}	0.39	0.40	0.51	0.30	1.12	0.30	1.14	1.65	1.60	1.13	1.97	2.59	0.39
Mn	0.00	0.01	0.01	0.00	0.27	0.00	0.24	0.01	0.01	0.01	0.02	0.00	0.01
Mg	0.56	0.54	0.46	0.66	0.24	0.67	0.26	0.17	0.19	0.23	0.04	0.00	0.31
Ca	0.00	0.00	0.00	0.00	0.00	0.00	0.01	0.00	0.00	0.00	0.00	0.00	0.00
Na	0.00	0.00	0.00	0.00	0.00	0.00	0.00	0.01	0.00	0.00	0.00	0.02	0.00
K	0.00	0.00	0.00	0.00	0.00	0.00	0.00	0.00	0.00	0.00	0.00	0.00	0.00
Ni	0.00	0.00	0.00	0.00	0.01	0.00	0.01	0.01	0.01	0.00	0.01	0.00	0.00
Σ cation	2.98	2.98	2.99	2.99	3.18	2.99	3.18	3.27	3.25	3.12	3.34	3.54	2.90

% Oxides	P4-2	P4-4	P1A-1	P1A-3	P1B-1	MB A-1	MB A-2	MB A-3	MB A-4	HR16A-1	HR16A-2	HR16B-1	HR16B-2
SiO_2	0.027	0.000	0.000	0.063	0.007	0.053	0.060	0.056	0.000	0.000	0.000	0.059	0.069
Al_2O_3	7.477	0.097	1.010	0.457	0.844	31.079	30.137	30.247	30.606	8.539	5.838	8.987	6.726
TiO_2	0.162	0.260	1.022	0.496	0.913	0.073	0.048	0.035	0.025	0.092	0.152	0.123	0.136
FeO	45.541	59.159	48.206	43.610	46.999	18.805	18.715	18.837	23.773	37.734	40.163	37.136	39.462
MnO	0.433	0.444	0.562	0.538	0.561	0.140	0.166	0.136	0.190	0.325	0.342	0.282	0.324
MgO	4.789	2.486	2.815	1.966	2.443	14.295	13.399	13.978	10.715	5.946	4.322	6.366	4.940
CaO	0.017	0.013	0.000	0.000	0.000	0.003	0.000	0.001	0.000	0.012	0.001	0.000	0.007
Na_2O	0.000	0.000	0.251	0.000	0.000	0.000	0.021	0.000	0.049	0.000	0.000	0.000	0.119
K_2O	0.000	0.000	0.000	0.000	0.000	0.000	0.000	0.004	0.027	0.000	0.000	0.000	0.000
NiO	0.240	0.310	0.198	0.061	0.145	0.143	0.113	0.203	0.112	0.165	0.185	0.147	0.105
Cr_2O_3	39.397	32.408	43.372	48.631	44.146	36.337	36.213	36.031	33.743	43.772	46.677	43.105	45.238
PROBE Σ	98.082	95.176	97.436	95.852	96.058	100.929	98.872	99.526	99.240	96.585	97.680	96.205	97.026
Fe^{3+}	24.81	32.89	26.80	12.12	13.07	5.23	5.20	5.24	6.61	10.49	11.17	10.32	10.97
Fe^{2+}	23.23	29.58	24.10	32.71	35.25	14.10	14.04	14.13	17.83	28.30	30.12	27.85	29.60
$\%Fe^{3+}$	0.49	0.50	0.50	0.25	0.25	0.25	0.25	0.25	0.25	0.25	0.25	0.25	0.25
Total	100.58	98.49	100.13	97.04	97.37	101.45	99.40	100.06	99.91	97.64	98.80	97.24	98.13
Si	0.00	0.00	0.00	0.00	0.00	0.00	0.00	0.00	0.00	0.00	0.00	0.00	0.00
Al	0.31	0.00	0.04	0.02	0.04	1.07	1.06	1.05	1.09	0.36	0.25	0.38	0.29
Ti	0.00	0.01	0.03	0.01	0.03	0.00	0.00	0.00	0.00	0.00	0.00	0.00	0.00
Cr	1.08	0.97	1.24	1.48	1.35	0.84	0.85	0.84	0.80	1.24	1.33	0.38	0.29
Fe^{3+}	0.65	0.94	0.73	0.35	0.38	0.11	0.12	0.12	0.15	0.28	0.30	0.28	0.30
Sum^{3+}	2.04	1.93	2.05	1.87	1.79	2.02	2.03	2.02	2.04	1.88	1.89	1.88	1.88
Fe^{2+}	0.67	0.94	0.73	1.05	1.14	0.34	0.35	0.35	0.45	0.85	0.91	0.83	0.89
Mn	0.01	0.01	0.02	0.02	0.02	0.00	0.00	0.00	0.00	0.01	0.01	0.01	0.01
Mg	0.25	0.14	0.15	0.11	0.14	0.62	0.59	0.62	0.48	0.32	0.23	0.34	0.26
Ca	0.00	0.00	0.00	0.00	0.00	0.00	0.00	0.00	0.00	0.00	0.00	0.00	0.00
Na	0.00	0.00	0.02	0.00	0.00	0.00	0.00	0.00	0.00	0.00	0.00	0.00	0.01
K	0.00	0.00	0.00	0.00	0.00	0.00	0.00	0.00	0.00	0.00	0.00	0.00	0.00
Ni	0.01	0.01	0.01	0.00	0.00	0.00	0.00	0.00	0.00	0.00	0.01	0.00	0.00
Σ cation	2.98	3.03	2.97	3.06	3.09	2.99	2.98	2.99	2.98	3.06	3.05	3.06	3.06

https://doi.org/10.1017/S0016756811000422 Published online by Cambridge University Press

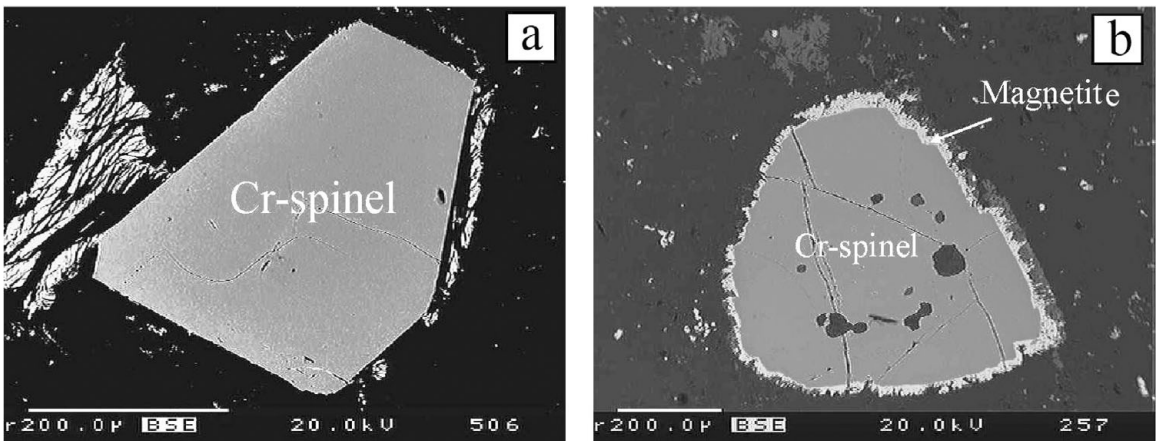

Figure 4. Protogranular textures with (a) characteristic linear grain boundaries; (b) characteristic curvilinear grain boundaries.

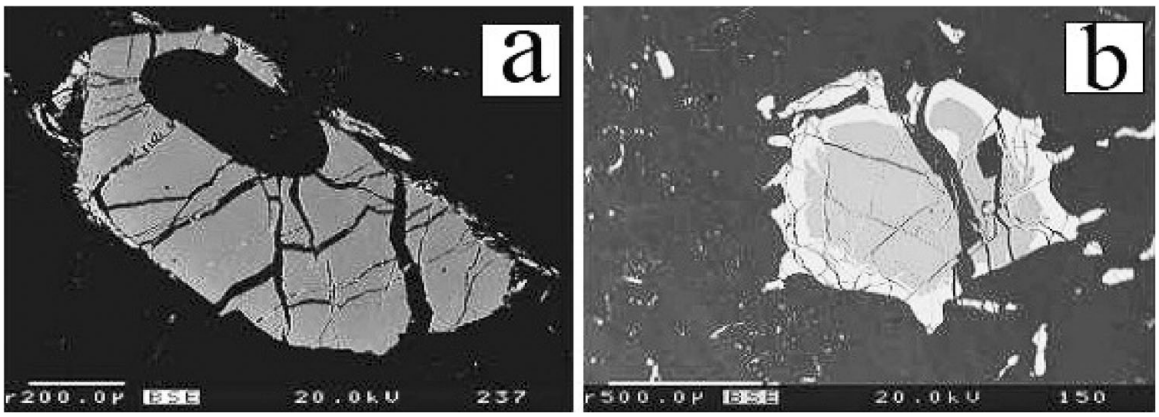

Figure 5. Cr-spinel shows heteradcumulate (a) and amoeboidal textures (b).

to differentiate between these trends. The first trend is Fe^{3+}-for-Cr^{3+} replacement and the second is Cr^{3+}-for-Al^{3+} replacement. Feasibility of trend recognition using both compositions and BSE imaging is facilitated by the tendency of the crystal chemistry portrayed by the studied Cr-spinels, with low atomic number elements Mg (AN = 12) and Al (AN = 13) co-varying with higher atomic number elements Cr (AN = 24) and Fe (AN = 26) (Fig. 6). Thus zones of different $MgAl_2O_4$ and $Fe(Cr, Fe^{3+})_2O_4$ show a large BSE contrast. Lines of constant average atomic number for the Al–Cr–Fe ternary diagram are shown in (Fig. 8c) and may be thought of as lines of constant BSE imaging. Trend 1 is almost parallel with these lines, whereas Trend 2 crosses them (Figs 7, 8). The primary Cr-spinel seems to follow the latter. Note the large contrast in electron back-scattering response between points p1 and p3 for P4A, and p2 and p3 for M8A in Figure 8. This verifies the large difference in composition.

5. Discussion: petrogenesis, metamorphism and tectonic aspects

The chemical zonation in Cr-spinel is attributed to pre-serpentinization metamorphism. Since magnetite occupies the outermost part of rimmed spinels it will not be tabulated in this study to determine its petrogenetic origin (Dick & Bullen, 1984; Barnes & Roeder, 2001). It seems that the primary spinel is affected by pre-serpentinization metamorphism, which is attributed to more involvement of subsolidus element redistribution during metamorphism involving major silicate phases, mainly olivine. Our analysis shows a temperature-dependent chemical gap (i.e. spinel solvus, Fig. 8a) between the Al-rich core (i.e. aluminium chromite and/or chrome spinel) and the Al-poor rim spinel (i.e. ferritchromite and magnetite) in some of the serpentinites studied (i.e. MBA, R8, HS12 and G9A). On the other hand, the Al-poor spinel (i.e. ferritchromite) completely replaces the primary one, with a continuous chemical shift from Cr-rich core to Fe^{3+}-rich rim (samples HR16, PZ1, M8A, P4A and P1A). Accordingly, large portions of the peridotites studied have been metamorphosed and primary spinel compositions partly or completely obscured by a veil of metamorphic effects. Based on the degree of metamorphism, the spinels can be divided into two categories where metamorphic spinel (including magnetite rims) is treated as a separate category (Fig. 9). The first is the primary Cr-spinel which is composed of Cr no. (Cr/(Cr + Al)) = 0.37–0.66, while the second is metamorphic Cr-spinel which consists mainly of Cr no. = 0.70–1.0 (Fig. 9).

https://doi.org/10.1017/S0016756811000422 Published online by Cambridge University Press

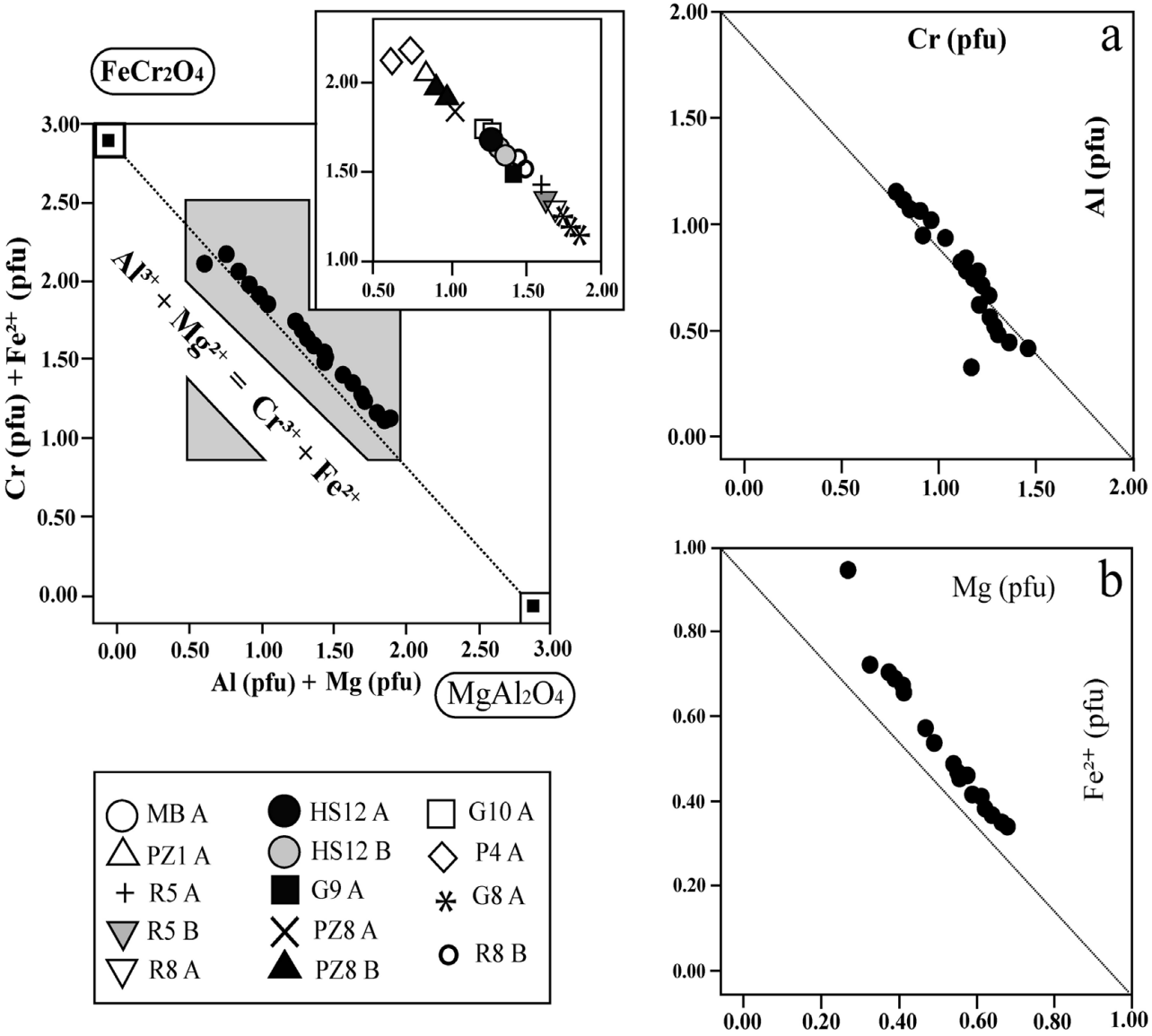

Figure 6. Cation plot for primary Cr-spinel. (a) Cr^{3+} and Al^{3+} calculated on the basis of two cations on the trivalent site. The diagonal line represents a 1:1 replacement; (b) Mg^{2+} and Fe^{2+} calculated on the basis of one cation on the divalent site. The plots show clearly a 1:1 replacement of $MgAl_2O_4$ by $FeCr_2O_4$.

5.a. Primary Cr-spinel

Disseminated Cr-spinels occur not only as a primary phase of chemically homogeneous, mainly, tectonites but also as both a cumulus and an intercumulus phase in ultramafic cumulates. The chemical variations of primary spinels of upper-mantle peridotite are interpreted as being the result of either different degrees of partial melting of the host peridotites (Luobusa trend) or caused by magma–mantle interactions (Dazhuqu trend). The Luobusa trend, however, is defined as a progressive decrease in Mg no. with increasing Cr no., while the Dazhuqu trend is distinguished by rapid Mg no. decrease with increasing Cr no. (Cannat *et al*. 1997; Hebert, Hekinian & Bideau, 1997). The composition of primary spinels in the studied serpentinites indicates that they have chemical affinity to both the Luobusa and the Dazhuqu trends (Fig. 10). Nevertheless, both Galalah (G8, G9 and G10) and Rayat (R5 and R8) serpentinites show large compositional spectra but with unambiguous affinity to the Luobusa trend (Fig. 10).

5.b. Metamorphic spinels and significance of Cr-spinel zoning

As mentioned earlier, the accessory spinels in serpentinite are found as zoned crystals. BSE images show three compositional zones from core to rim: (a) a homogeneous core that normally retains the primary Cr-spinel composition. This is surrounded by (b) an Al- and Mg-poor zone of 'ferritchromite' that changes composition gradually towards magnetite at the margin (e.g. M8, Fig. 11). Owing to the continuous change of the chemical composition of the spinel during metamorphic alterations, the record of maximum *P*–*T* conditions of the primary Cr-spinel composition is largely erased or veiled. In most cases, it has

https://doi.org/10.1017/S0016756811000422 Published online by Cambridge University Press

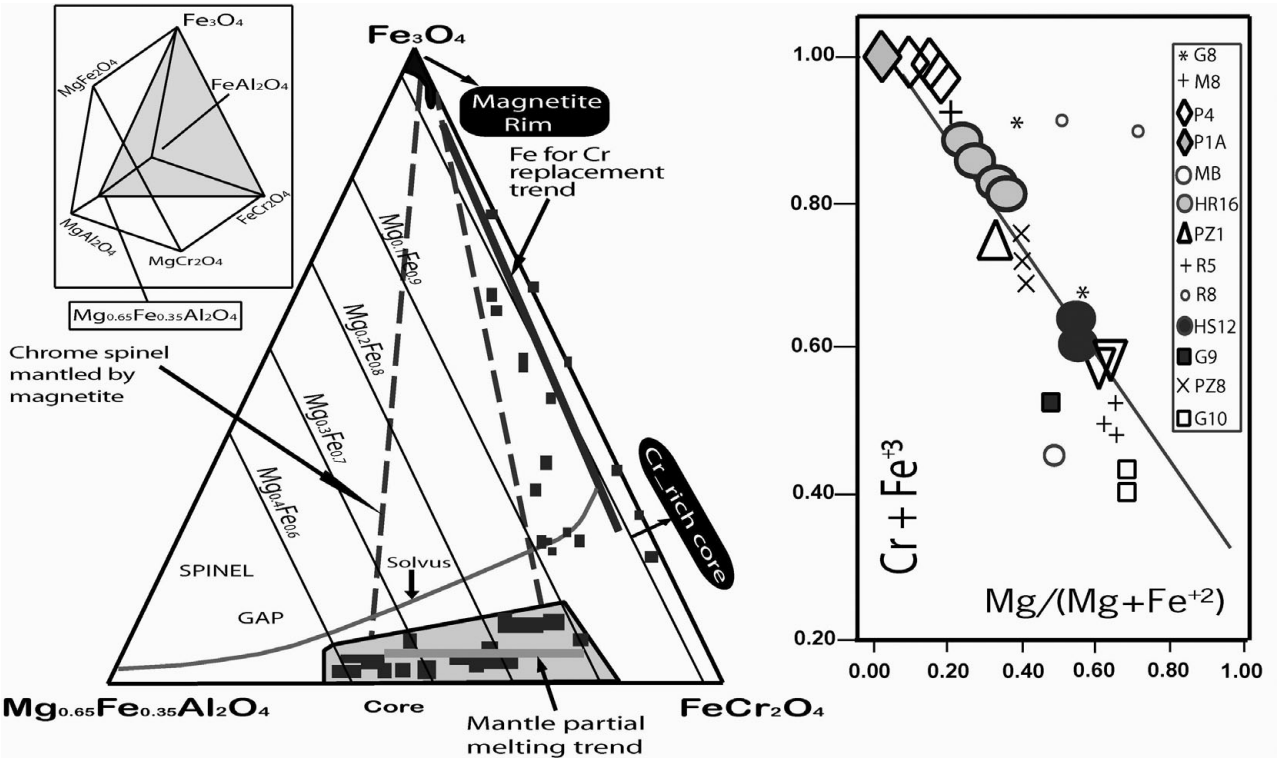

Figure 7. Projections of the oxidized spinel prism of the entire dataset for the Cr-spinel studied. Lines with arrows show zoning trends.

undergone complex metamorphism, transforming it into a chemically heterogeneous ferritchromite. In some cases, zoning in ferritchromite is intergrown with (c) the aluminous phase chlorite, which forms a spongy texture around the primary spinel. However, it is unclear whether spinel metamorphism preceded or followed serpentinization, and hence the compositional trends in the 'ferritchromite', which are in contrast to primary chromite, could help solve this problem. However, chrome spinels have undergone subsolidus re-equilibration as a result of solid–solid and solid–liquid reactions during cooling, hydrothermal activity and serpentinization of the host rock. It is important to consider these factors in order to determine the extent of chemical change in the chrome spinel. Therefore, when using chrome spinel in provenance and petrogenetic studies of dismembered, deformed and serpentinized ultramafic complexes, some or all of these factors should be assessed.

5.c. Syn- and post-serpentinization spinel metamorphism

Magnetite was formed along the margins and cracks of Cr-spinel grains throughout the alteration either as a result of replacement or nucleation or both. Inspection of Figure 4a clearly shows that primary Cr-spinel with a euhedral outline and a thin magnetite rim is being defined by diffusive replacement of Mg^{2+} and Al^{3+} by Fe^{2+} and Fe^{3+} in the spinel structure resulting in higher average mass number, or lighter shades on BSE images of magnetite overgrowth. In Figure 2b, however, magnetite has ragged non-idiomorphic grain boundaries against enclosing serpentine. The Cr-spinel–magnetite contact might be interpreted to be an overgrowth and to a lesser extent formed by replacement, favouring nucleation as the likely mechanism for the increase in spinel grain size during alteration. The magnetite rims are nucleated irregularly away from the Cr-spinel rims and join the magnetite stringers of the serpentine matrix (Fig. 5b). But the presence of chlorite aureoles (see Fig. 2b) as a buffer between the magnetite rim and enclosing serpentine may advocate that the diffusive replacement is also manifested in the formation of an accretionary magnetite rim.

Generally, the alteration of Mg–Al-rich spinel was a replacement process in which Fe^{2+} and Fe^{3+} from the magnetite rimming primary Cr-spinel was substituted by MgO, Al_2O_3 and, to a lesser extent, by Cr_2O_3. It is important to underline that the dissolution of Cr is favoured in a reducing environment whereas reprecipitation occurs under locally oxidizing conditions. After the release of Mg and Al during the alteration, primary Cr-spinel interacted with serpentine, producing chlorite aureoles. The primary Cr-spinel alteration suggests that the alteration occurred in greenschist facies. However, the serpentinization produces rims of secondary magnetite grown around Cr-spinel (Fig. 5b), making it possible that ferritchromite may be either formed by regionally metamorphosed terranes or due to a decompression metamorphic regime accompanied by a diapiric rise of serpentinite bodies. The decompression metamorphic regime, however, is related to severe decompression–exhumation caused by return flow of hydrated peridotite protoliths above the sinking slab. Nevertheless, chlorite-ferritchromite forms as a

https://doi.org/10.1017/S0016756811000422 Published online by Cambridge University Press

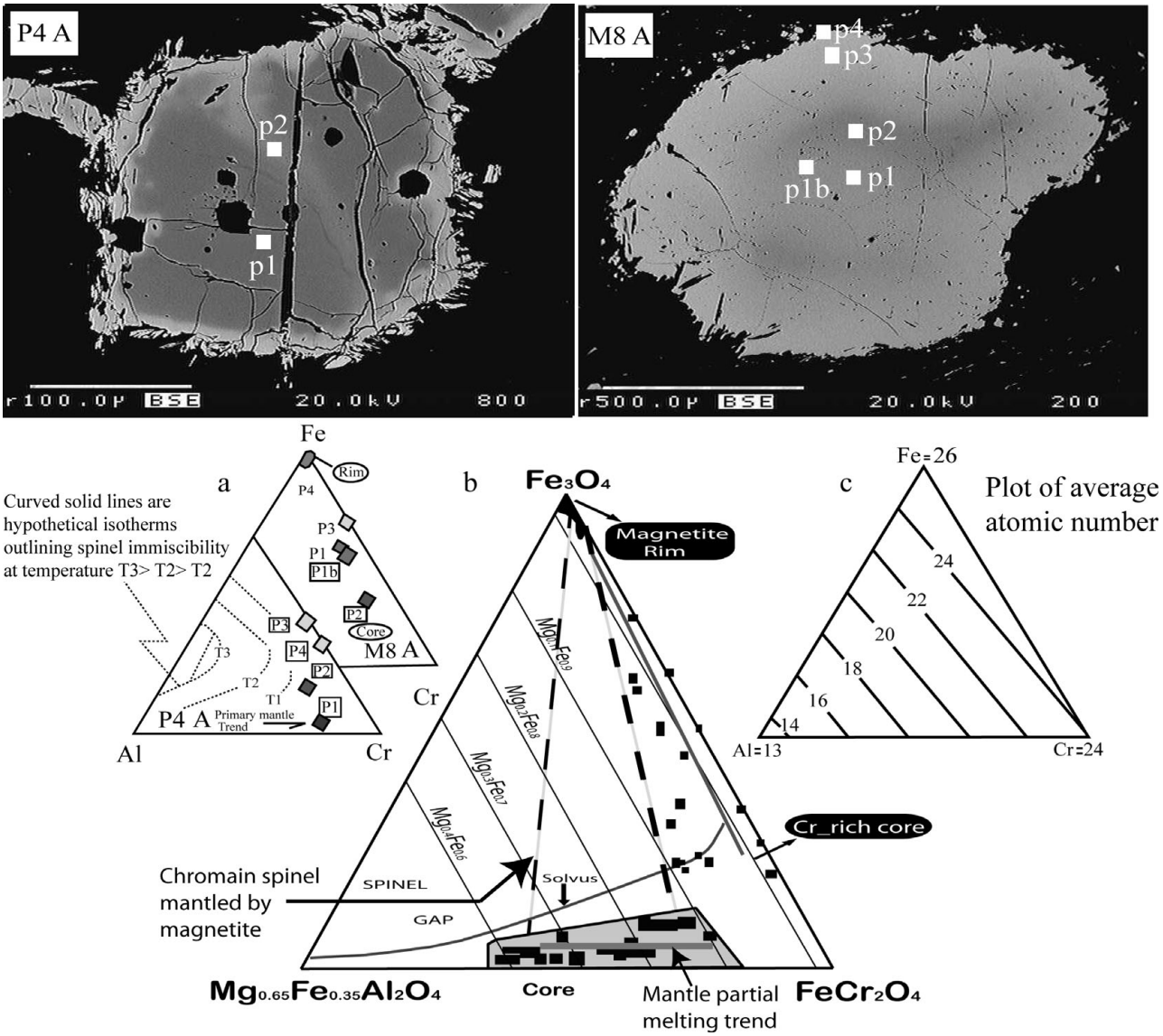

Figure 8. (a, b) Projections of the oxidized spinel prism for MOA PÅ and entire dataset. Arrowed lines show zoning trends. Lower-case letters (p1, p2, etc.) indicate analyses for points on the BSE images. Upper-case letters indicate Fe-for-Cr replacement trend and mantle partial melting trend analyses for points on the BSE images. (c) Ternary diagram showing lines of constant average atomic number for Al, Cr and Fe.

result of the interaction between primary Cr-spinel, magnetite and serpentinite. Taking into consideration the undersized serpentinite exposure, decompression metamorphism is the more adequate explanation in the elucidation of the Cr-spinel zoning. Unlike the accompanied pre-serpentinization silicates, the Cr-spinel is a ubiquitous accessory mineral and it is characterized by the retention of metamorphic memory during an overprinting metamorphic episode under a multistage retrograde uplift–cooling and exhumation of the serpentinized peridotites. In regionally metamorphosed terranes, the spinel is present in the form of chrome magnetite in low-grade serpentinites, ferritchromite in antigorite serpentinites and chromite in talc-olivine rocks (Evans & Frost, 1975). This regional metamorphic succession can be easily tracked in the field. Nevertheless, the zonation displayed by the spinel in a decompression metamorphic regime under a continuing exhumation mechanism might reveal complex metamorphic evolution paths that include pre-serpentinization, high-temperature (> 300–400 °C) syn-serpentinization and/or post-serpentinization spinel metamorphism. It seems likely that all talc in talc-olivine rocks has probably fully reacted away during the decompression metamorphism; this 'high temperature' variant of serpentinization cannot really be proved. It might be concluded that the serpentinization process reached an advanced stage owing to continued low temperature fluid–rock interaction under oxidizing conditions, where only serpentine and magnetite were present. Determining the metamorphic evolution of these rocks, which consist of only two phases, is rather difficult, because fluid–mineral phase relationships cannot always be employed. Therefore, magnetite that occupies the outermost rim around pre-existing spinel grains is considered to be due to the effect of post-serpentinization reactions. Consequently, the post-serpentinization spinel metamorphism is not

https://doi.org/10.1017/S0016756811000422 Published online by Cambridge University Press

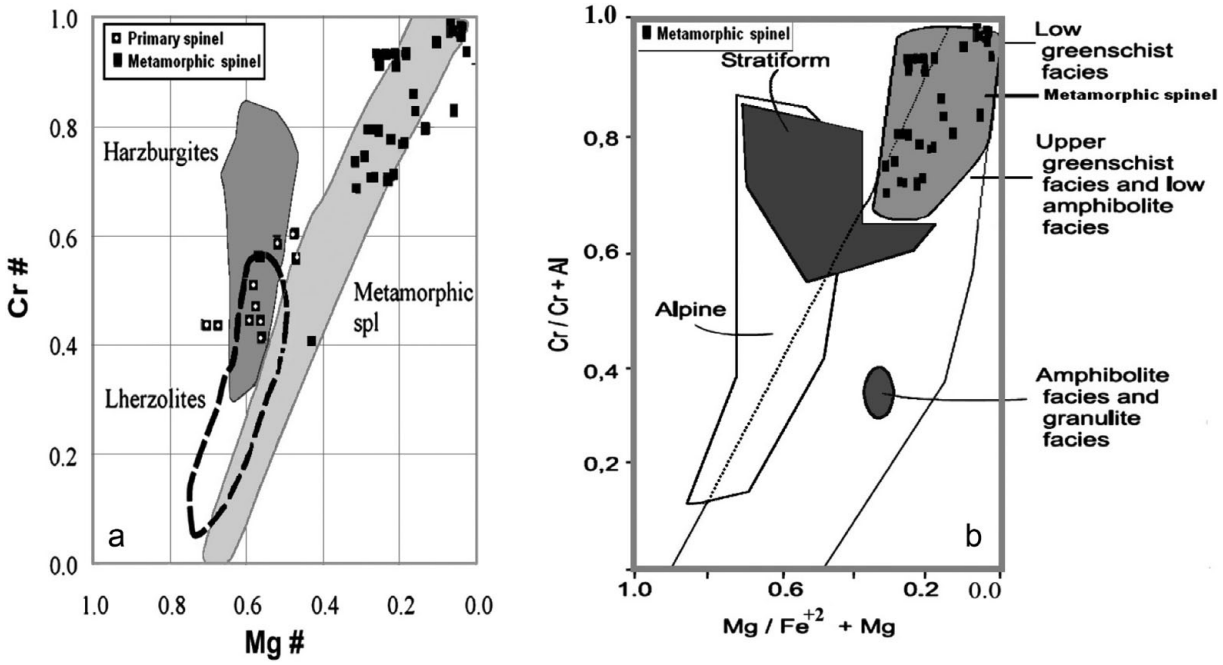

Figure 9. (a) Cr no. v. Mg no. diagram showing the chemical composition of primary and metamorphic spinels (compositional fields after Stevens, 1944); (b) Cr no. v. Mg no. for metamorphic spinel compared with other tectonic associations (Irvine, 1967).

considered in this study because it took place at the final stage of the decompression metamorphic regime accompanied by a diapiric rise of the serpentinite bodies (N. Aziz, unpub. Ph.D. thesis, Sulaimani Univ., Iraq, 2008).

Referring to the petrographic study, the Al-rich chromites which show textural evidence of partial replacement by ferritchromite, i.e. anhedral shapes and embayments, indicate that alteration advanced from all directions, outwards towards the margin of the grains (e.g. M8 in Fig. 11). The anhedral primary Cr-spinel is always surrounded by a chemically and optically well-defined ferritchromite. There are some exceptions that include serpentine and chlorite minerals forming a spongy/chessboard texture. This suggests that ferritchromite formed as a polycrystalline aggregate that allowed communication between the growing ferritchromite and the partially or completely dissolving spongy cores. Part of the Cr_2O_3 was incorporated in the magnetite rims (1 wt % Cr_2O_3), distinguishing them from the anhedral, ragged magnetite disseminated in the main mass of serpentine which do not contain Cr_2O_3. Note that the abrupt change in electron back-scattering at the magnetite–primary Cr-spinel interface may indicate that the spinel solvus was intersected by this spinel (Figs 7, 8).

5.d. Pre-serpentinization spinel metamorphism

The Fe–Mg partitioning between olivine and spinel is frequently used to derive temperature estimates for peridotites (Irvine, 1967; Jackson, 1969; Fabriès *et al*. 1989; Roeder, Campbell & Jamieson, 1979; O'Neill, 1981; O'Neill & Wood, 1979; Sack & Ghiorso, 1991). Applying this technique to peridotites is problematic because of possible subsolidus re-equilibration down to 500 °C that severely affects the Fe–Mg distribution between olivine and spinel (Lehmann, 1983). Using the Fe–Mg partitioning leads to unreasonably low temperature estimates for olivine–Cr-spinel pairs with assumed Fo in olivine = 90. The Fe–Mg subsolidus re-equilibration under low *P–T* conditions might cause a gradual shift in the chemical composition of primary spinel towards ferritchromite. In some of the serpentinites studied, the existence of primary Cr-spinel may indicate an incomplete reaction. The presence of minerals stable at lower temperatures such as chlorite and serpentinite also indicates that the lherzolite rapidly cooled down below the nucleation cut-off temperature. Fe–Mg exchange thermometry applied to coexisting olivine and spinel in these rocks shows that they were equilibrated between 600 °C and 800 °C (Fig. 12). The spectrum of Cr-spinel compositions in the studied serpentinites was compared with spinel trends in equilibrium at various temperatures, and olivine having a composition that encompassed the range expected in mantle tectonites. Olivine–spinel equilibrium temperatures are 700 °C and 800 °C for primary spinels 1 and 2 with the same calibration. The Cr-spinels were unequally divided into primary spinels 1 and 2. These different calibration temperatures, however, might have depended on the rate of decompression.

6. Tectonic implications

Serpentinite occurs in several active tectonic settings. These include mid-oceanic ridges and transform faults (Cannat, Bideau & Bougault, 1992; Michael *et al*.

https://doi.org/10.1017/S0016756811000422 Published online by Cambridge University Press

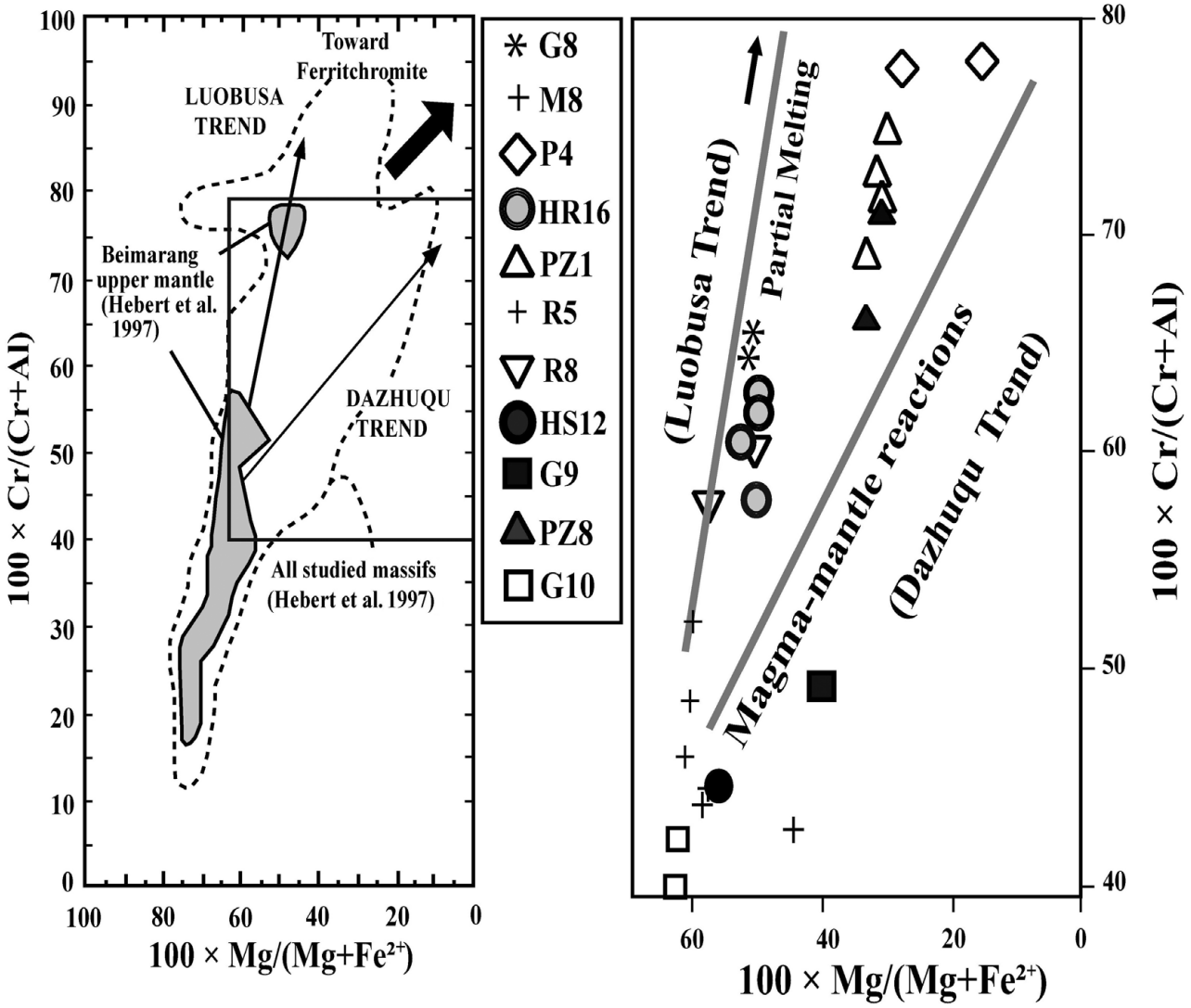

Figure 10. Primary spinels of the serpentinites studied compared with the Luobusa and Dazhuqu trends.

2003), submarine magma-poor continental rifts (Nicolas, 1985; Boillot *et al*. 1989; Whitmarsh, Manatschal & Minshull, 2001) and subduction zones (Fryer, 1992). The tectonic regimes where serpentinites occur possess the petrological characteristics, original types of protolith and mode of emplacement (Alt & Shanks, 2003). In the case of completely serpentinized ultramafic rocks (i.e. serpentinite mélange) that preserve no primary silicate minerals, the composition of unaltered primary Cr-spinel (which preserves its compositional signature after the serpentinization) may provide useful petrotectonic information. The chemistry of Cr-spinel plays an important role in classifying mantle-derived peridotites by origin and tectonic setting. Cr-spinel composition is extensively used as a petrogenetic and geotectonic indicator (Irvine, 1967; Dick & Bullen, 1984; Arai, 1992, 1994; Proenza *et al*. 2004). Regardless of metamorphism, the cores of Cr-spinel grains preserved the Cr-spinel primary chemical composition trend (Trend 1). This trend is common in least metamorphosed chrome spinel (Roeder, Campbell & Jamieson, 1979). It is characterized by low-Fe^{3+} (high-Al), and often represents primary spinel composition (Quick & Gregory, 1995) (Fig. 9a). The Fe^{3+} is concentrated in chrome spinel and is attributed to low-temperature redistribution with surrounding serpentinized olivine. Cation ratios (i.e. Cr no. and Mg no.), however, could change subtly depending on physicochemical conditions (Irvine, 1967). For this reason, such variations must be assessed using Figures 9a and 11 before interpreting spinel compositions as petrogenetic indicators in the present study. Figure 13 shows that the tectonic affinities of the studied samples are within the fore-arc setting of peridotite protoliths. Generally, the peridotites of the Zagros ophiolite have high-Cr no. spinel compositions that mostly plot in the fore-arc field (Moghadam & Stern, 2010). The similarities between Cr no. spinel compositions of the studied samples and the peridotites of the Zagros ophiolite validate the conclusion that a broad and continuous tract of fore-arc lithosphere was created during Late Cretaceous time (Moghadam & Stern, 2010). As stated in Section 2, the Qulqula Radiolarite lies structurally beneath the serpentinite mélange and above the Arabian

https://doi.org/10.1017/S0016756811000422 Published online by Cambridge University Press

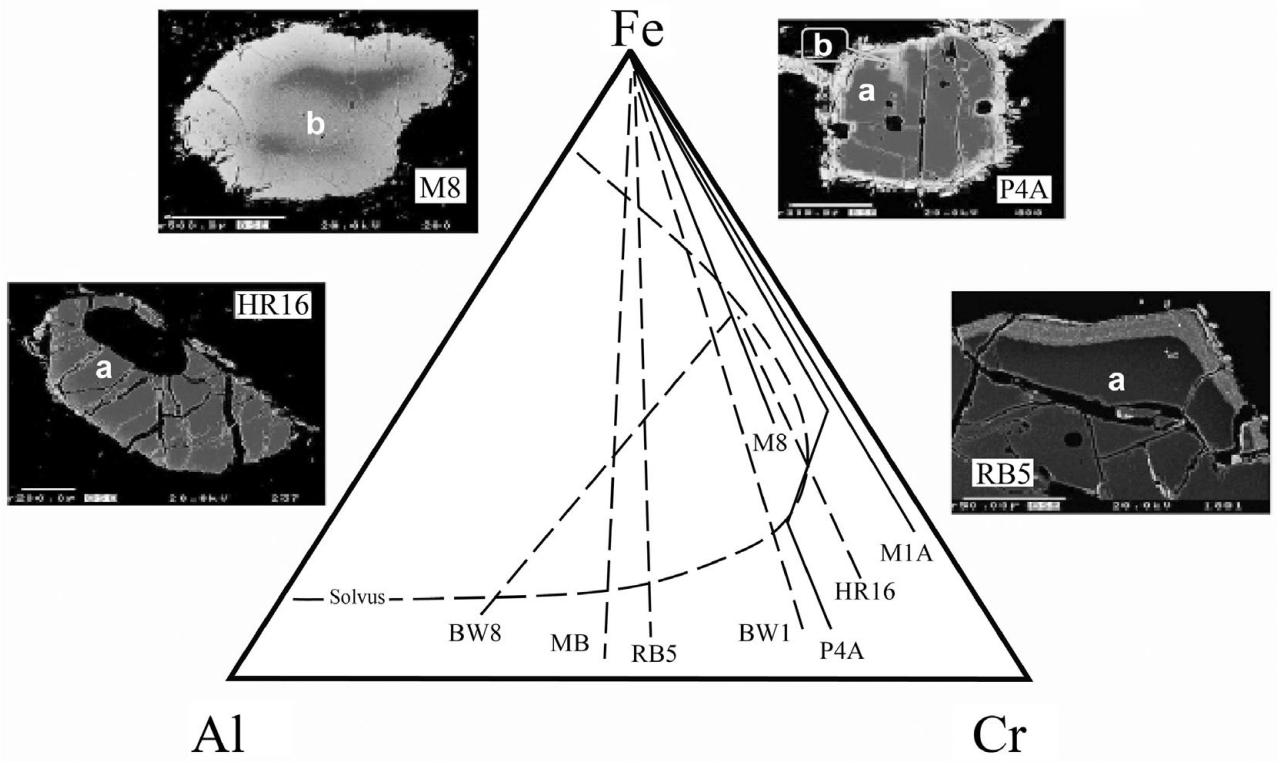

Figure 11. Al–Cr–Fe ternary diagram in conjunction with back-scattered image of Cr-spinel grains illustrating three different compositional zones from core to rim: (a) homogeneous core that normally retains the primary Cr-spinel composition (dark grey) surrounded by (b) Al-and Mg-poor zone of ferritchromite (light grey) that changes gradually in composition towards magnetite at the margin (white). Mawat serpentinite, sample M8 primary spinel composition is completely obscured by a pre-serpentinization metamorphic veil.

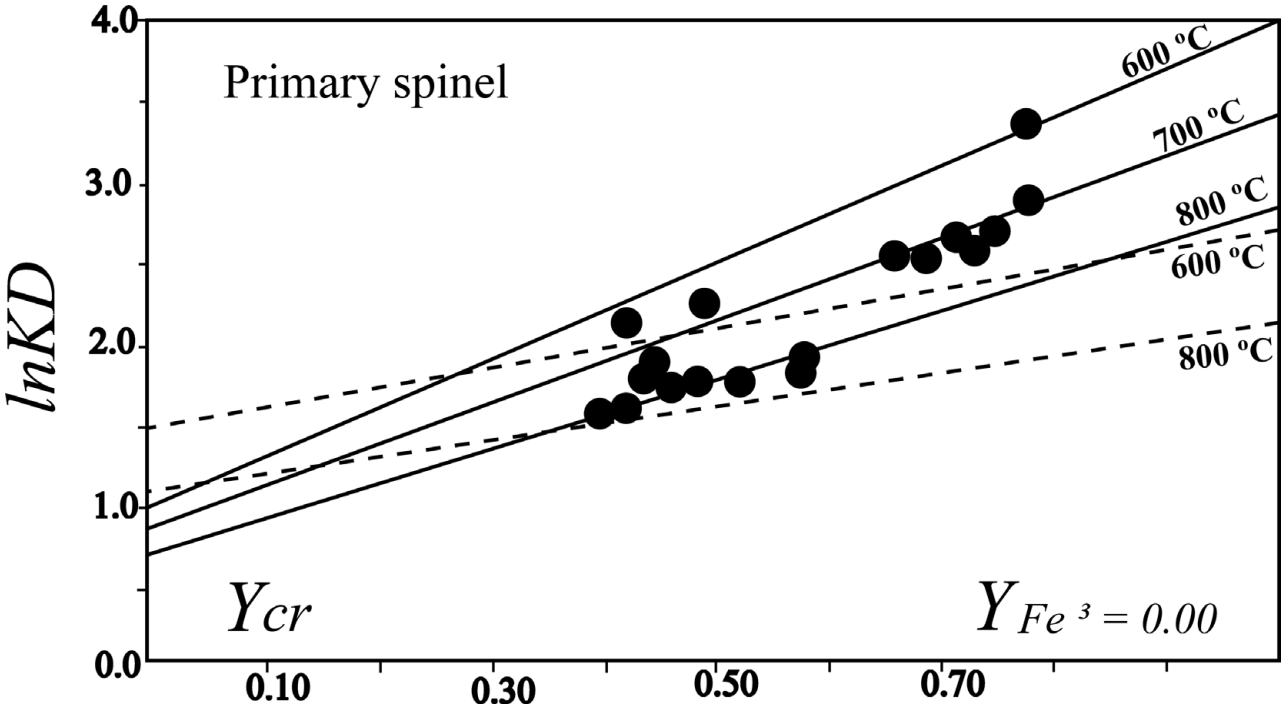

Figure 12. Plot of lnKD v. Y_{Cr}; lnKD = $(X_{Mg}/X_{Fe})Ol \times (X_{Fe}/X_{Mg})Sp$; Y_{Cr} = Cr/(Cr + Al). Solid lines are the isotherms calculated from the equation of Fabriès *et al*. (1989); dashed lines are calculated using the equation of Roeder, Campbell & Jamieson (1979); olivine (Fo = 90) is assumed to be in equilibrium with spinel; accuracy is within + 50 °C. Primary spinel 2 is equilibrated with olivine at 700 °C (i.e. P and PZ).

platform carbonate of Balambo. There is no doubt that radiolarian cherts of the Qulqula sequences are oceanic in origin and very possibly from basins of great depth. The sequences, however, were deposited in a narrow basin extending from Oman (Hawasina series) in the south, continuing northward into south Iran (Pichakun series), western Iran (Kermanshah), the Kurdistan Region and NE Iraq (Qulqula), ending

https://doi.org/10.1017/S0016756811000422 Published online by Cambridge University Press

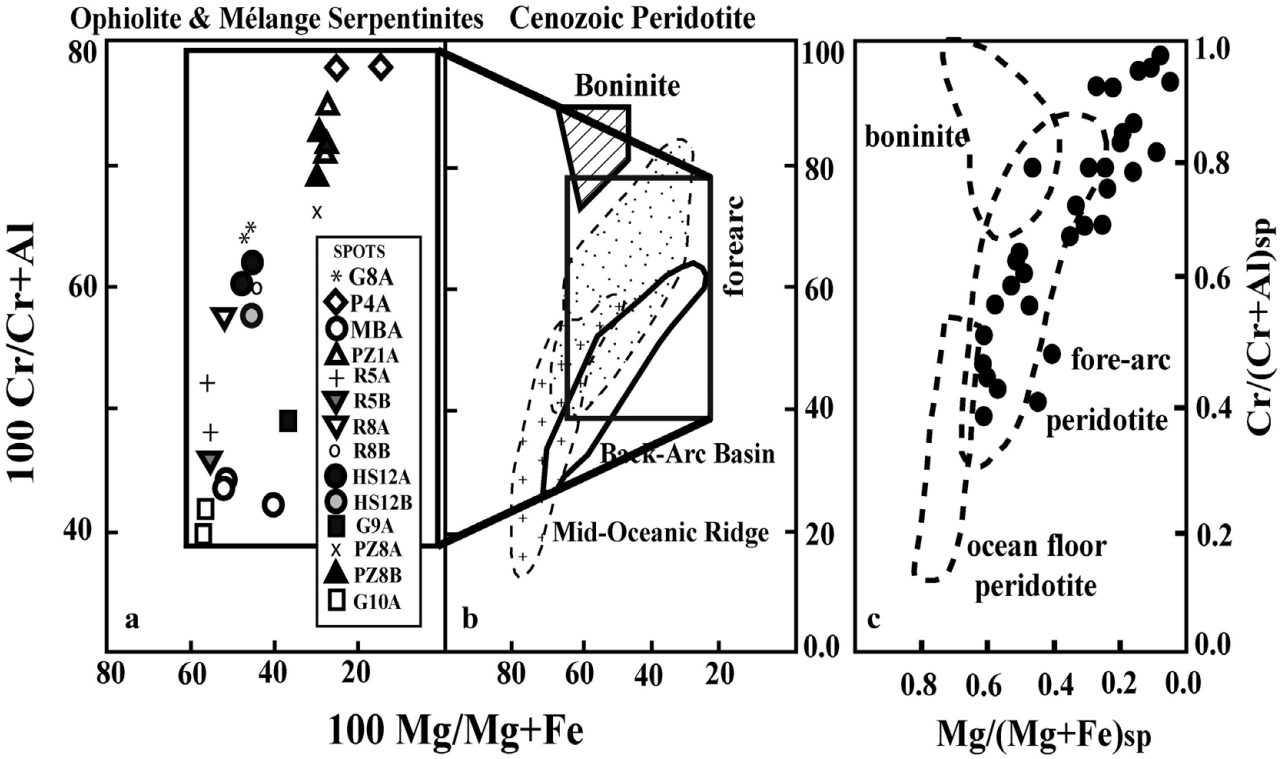

Figure 13. Composition of primary spinels in studied ophiolitic-serpentinite associates and mélange serpentinites, (a) compared with those in modern peridotites; (b) data on 100Cr/(Cr + Al) (Cr no.) v. 100Mg/(Mg + Fe) (Mg no.); diagram modified after Dick & Bullen (1984). Most spinels studied have a high Cr no., suggesting peridotite protoliths formed in a fore-arc setting; (c) Cr no. v. Mg no. diagram for chrome spinel compositions of Zagros Suture Zone serpentinites. The majority of the data also suggest a fore-arc setting (Dick & Bullen, 1984; Arai, 1994), fore-arc (Parkinson & Pearce, 1998) and boninites (Arai, 1994; Barnes & Roeder, 2001).

in Turkey (Kocali series), and bordering the Arabian platform carbonates (e.g. Balambo Formation, Albian–Cenomanian). Hence, the sequences clearly define the continental margin of the Arabian plate and are largely preserved within the Zagros Suture Zone. The age of the radiolarite sequences of Qulqula is controversial and has not yet been precisely determined. This has been suggested to be owing to the intricate folding and faulting of the sequences (Buday, 1980). Such structural characteristics of Qulqula are anticipated as a result of actively deformed accreted sediments. Further to the south of the studied area, the Kermanshah radiolarites were recently dated by radiolarians to the Lower Pliensbachian for the oldest ones, up until the Turonian for the youngest (Gharib & De Wever, 2010). The radiolarite sequences (and serpentinite–matrix mélange) in the studied area form an accretionary-complex terrane with the Qulqula Radiolarite that adhered to the autochthonous carbonate of Balambo (Albian–Cenomanian). The Qulqula Radiolarite contains blocks varying in size and typically elongated with long axes parallel to the upper and lower contacts with the above-mentioned formations (i.e. Balambo and allochthonous thrusted sheets). These blocks are made of mafic–ultramafic and sedimentary rocks embedded in a fragmental matrix of incompetent fine-grained material. This internal disruption of the stratigraphy of the latter is best considered as a broken formation (i.e. tectonic mélange) rather than a true mélange, which shows sporadic or chaotic blocks of exotic origin embedded in a sedimentary matrix (Aziz, Aswad & Koyi, 2011). Field observations west of Penjween town and at the tectonic contact between the Qulqula (Lower Pliensbachian–Turonian; Gharib & De Wever, 2010) and Balambo (Albian–Cenomanian age; Jassim *et al*. 2006) formations show that the occurrence of blocks belonging to the latter in the former can easily be traced. Such a finding might facilitate the dating of the exhumation of the accretionary complex, which was presumably post-Turonian. Furthermore, the erosional products from the Qulqula Radiolarite and serpentinite mélange were shed as flysch deposits of the Tanjero Formation, which is equivalent in age to the Amiran Formation in Iran, and it is considered a typical peripheral foreland deposit which occurred on the Arabian passive margin. The Tanjero flysch formation was deposited in the foredeep where deeper-water marine sediments of Shiranish were deposited further to the west. The timing of the Arabia–Central Iran microplate continental collision is poorly constrained, and estimates range from Late Cretaceous to Late Miocene time (Fakhari *et al*. 2008; Horton *et al*. 2008; Omrani *et al*. 2008). The controversy about the timing of the collision is dealt with in this study by putting more emphasis on the presence of the serpentinite-derived terrigenous sediments in the mentioned flysch and molasse deposits. These deposits heralded the uplift that resulted from accretion due to subduction

https://doi.org/10.1017/S0016756811000422 Published online by Cambridge University Press

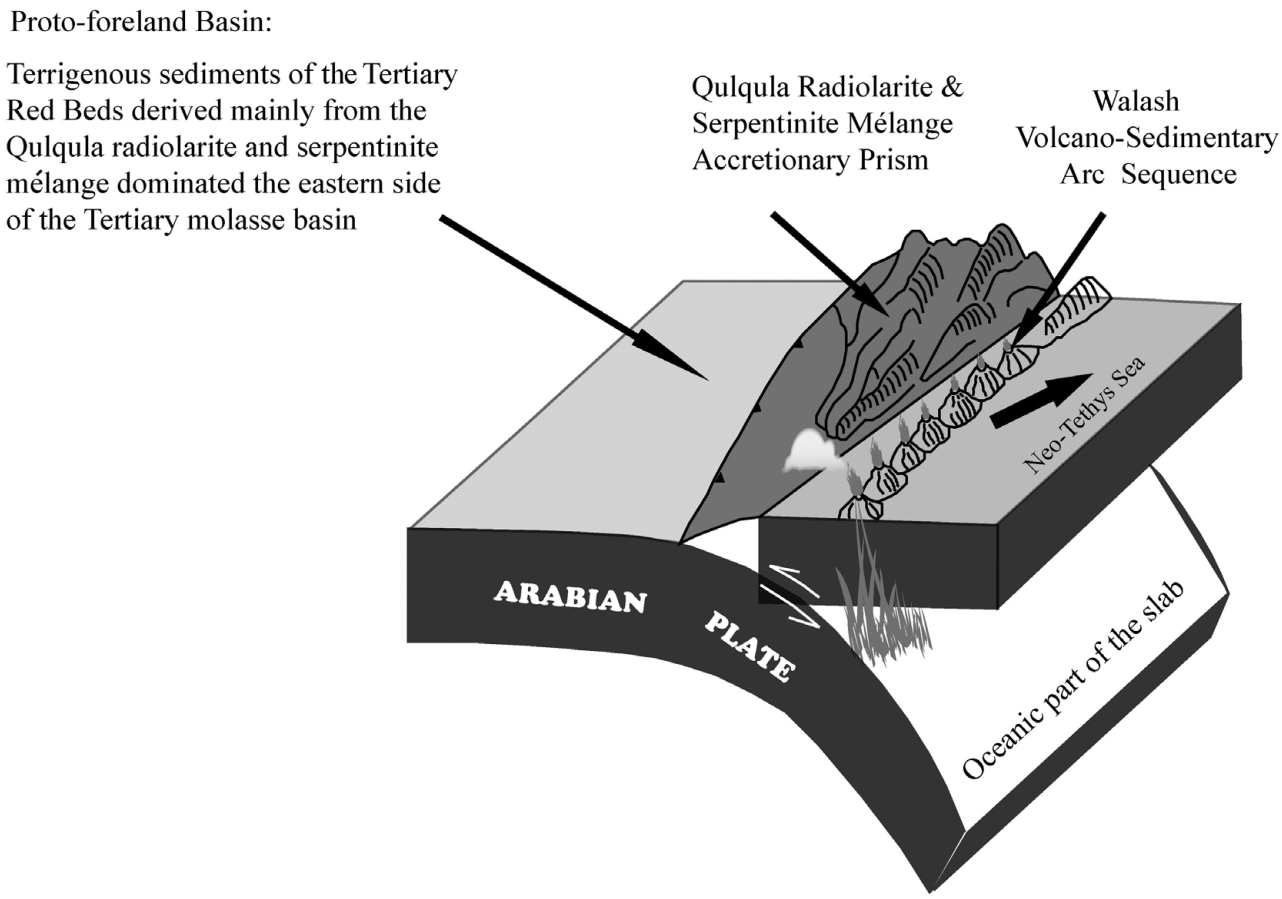

Figure 14. Schematic block diagram showing the postulated fore-arc setting and emplacement of serpentinite mélange (Paleocene–Eocene).

during Maastrichtian–Palaeogene time throughout the continuing convergency onto the margin of the Arabian plate. Hence, both the Qulqula Radiolarite and the serpentinite–matrix mélange are assumed to derive from the Late Mesozoic accretionary complex related to the eastward intra-oceanic subduction of the Neo-Tethys. The development of the intra-oceanic island arc is clearly supported by the ^{40}Ar–^{39}Ar geochronological data from the upper volcanics of Walash, which suggest that the late intra-oceanic arc activity continued through Palaeogene time and can be divided into an early phase of andesitic volcanism around 43.1 ± 0.3 Ma and a subsequent extensional-arc phase magmatism between 40.1 ± 0.3 Ma and 32.3 ± 0.4 Ma. Such a finding compels the conclusion that the final resorption of the 'oceanic arc' domain took place after 32.3 Ma. The Neo-Tethyan strand in the northwestern Zagros remained open into the Palaeogene (i.e. after major ophiolitic serpentinite mélange emplacement). The geochemistry of the volcanic unit of the Gemo sequence of the ophiolite-bearing Mawat thrust sheet (Upper Allochthon) advocates that the volcanic units are of an infant-arc affinity (Farjo, unpub. M.Sc. thesis, Mosul Univ., Iraq, 2006). It has a conformable lower contact with the Mawat ophiolite massif of Albian–Cenomanian age (118–97 Ma; Aswad & Elias, 1988). Further to the southeast of the Mawat nappe along the Zagros Suture Zone, basalt with calc-alkaline island arc affinity and arc-related volcaniclastic rocks (92.07 ± 1.69 Ma) has been found to be deposited unconformably above the Neyriz ophiolite (Babaie *et al*. 2001, 2006; Babaei, Babaie & Arvin, 2005). Babaie *et al*. (2001) suggest that the emplacement of the volcanic arc rocks adjacent to the thrust sheets of the crustal and mantle sequences of the Neyriz ophiolite was probably a result of subduction-related processes and the closure of the Tethys Ocean in Late Cretaceous time. The age data could indicate that both the Mawat and Neyriz ophiolites share the same palaeogeographic and tectonic history during Late Cretaceous time. Note that the nascent arc setting of the Mawat ophiolite is suggested to have been emplaced over a second subduction zone of Palaeogene age (i.e. dual subduction-zone model). In spite of that, the Palaeogene arc activity of Walash was coeval with the Urumieh–Dokhtar arc magmatic activity (Omrani *et al*. 2008); these two magmatic arcs almost certainly originate from the different slabs.

Based on the accretionary prism formation mode (Fig. 14), the emplacement of the serpentinite mélange may be synchronous with late flysch sedimentation of Tanjero. If so, the upper part of the accretionary prism corresponds to the Upper Maastrichtian (Fig. 14). Based on the above model and considering the tectonogenesis of primary chrome spinels, the subduction-accretion events are documented by the

https://doi.org/10.1017/S0016756811000422 Published online by Cambridge University Press

Late Mesozoic–Early Cenozoic, during which fore-arc-type sedimentary basins (i.e. Naopudan, Palaeogene) were separated from flexural foreland basins (e.g. Tertiary molasse basin) by these sedimentary and serpentinite mélanges (i.e. Qulqula Rise). It has been noted that at the very front of the Mawat thrust the nappe lies on Tertiary molasse (Tertiary Red Beds) whose limits tightly overlap with nappe outcrops, suggesting a close relationship between their deposition and progressive nappe emplacement (Aswad, 1999). Serpentinite mélanges, however, seal the thrust contact of the Lower Allochthonous sheet (43–32 Ma; A. Koyi, unpub. M.Sc. thesis, Mosul Univ. Iraq, 2006) of the nappe and the Miocene molasse unit, signifying that this thrust was emplaced pre $\sim$ 23 Ma (N. Aziz, unpub. Ph.D. thesis, Sulaimani Univ. Iraq, 2008). The Tertiary molasse, however, shows neither distinct alteration nor damage zones (i.e. metamorphic sole) below the thrust fault. Gravity sliding, however, is the only candidate mechanism that could explain such an emplacement process of the Mawat nappe (Aswad, 1999), which probably detached after collision and emplaced on Tertiary molasse in Late Oligocene (*c.* 25 Ma) time. Nonetheless, the timing of collision is not grossly in conflict with the proposed age of prior to 25–23 Ma in the northern Zagros (J. Omrani, unpub. Ph.D. thesis, Institut des Sciences de la Terre, Paris, 2008). The sliding displacement of the Mawat nappe (which is estimated to be less than 10 km) away from dextral strike-slip (Aswad, 1999) is due to protracted continental convergence (J. Omrani, unpub. Ph.D. thesis, Institut des Sciences de la Terre, Paris, 2008; Alvarez, 2010), which provided a structural high to facilitate gravity sliding of the nappe and hence structurally controlled molasse deposition in adjacent troughs (Aswad, 1999). Gravity sliding of the nappe is only possible if the rocks (i.e. serpentinite mélanges) are weak enough to sag and spread under their own weight. Therefore, the sliding surface developed almost entirely within a serpentinite mélange. Assuming this, the strength (or the weakness) of serpentinite mélange might differ owing to the variable amount of exotic blocks in the block-in-matrix structure or bimrock (Lindquist & Goodman, 1994). The influence of bimrock rheology on metamorphosed chrome spinel needs further investigation.

7. Conclusion

The compositions of the studied Cr-spinel, in conjunction with BSE imaging of Cr-spinel, indicate that the primary chrome spinel is altered along margins or cracks, showing continuous and/or discontinuous compositional variations to ferritchromite and magnetite. The chemical alteration is attributed to pre-serpentinization and/or syn- or post-serpentinization spinel metamorphism. These Cr-spinels show a wide range of Y_{Cr} from 0.37 to 1.0 and mainly low Ti content of $<$ 0.2 wt % TiO_2, while the X_{Mg} ranges from 0.0 to 0.75. Three stages have been recognized in the studied spinel: first (residual-mantle)-stage spinels are Al-rich, have very restricted Cr nos. of 0.40 to 0.65 and are more aluminous, with an Al_2O_3 content $>$ 20 wt % (Trend 1). The second-stage spinels are Cr-rich and have Cr no. values around $>$ 0.65 (Trend 2). Finally, the third stage exhibits a very narrow magnetite rim. The abrupt change in electron back-scattering at the magnetite–Cr spinel interface may indicate that the spinel solvus was intersected. Magnetite is frequently associated with serpentine polymorphs. These three stages represent primary Cr-spinel, pre-serpentinization spinel metamorphism and syn- or post-serpentinization spinel metamorphism, respectively. The second and third stages point to diachronous metamorphic paths resulting from continuous tectonic evolutions influenced by either slow or fast uplifting of mantle protoliths. Where the primary chrome spinels are flanked by a very narrow magnetite rim, the uplifting of mantle protolith is rather fast (i.e. the absence of slow decompression-related ferritchromite coronas between primary chrome spinels and magnetite rim). When Fe–Mg exchange thermometry was applied to coexisting olivine and spinel in these rocks, the result showed that pre-serpentinization spinel equilibrated at between 700 °C and 800 °C. The absence of either the first (residual mantle) stage or second stage may depend on the rate of decompression (i.e. diapiric uplifting). It is difficult to know precisely the tectonic environments of strongly hybridized rocks. This is because the mélange rocks varied in age and isotopic- and geochemical signatures. The tectonic affinity based on the chemical characteristics of primary chrome spinels is within the fore-arc setting of peridotite rootlets. The evidence suggests that fore-arc serpentinites contributed to exhumation of overlying rocks during active subduction starting in Late Maastrichtian time and during late pre-collisional activity.

Acknowledgements. We would like to thank Dr Zeki A. Al-Jubori for critical reading of an early draft of the manuscript. The authors also wish to thank Dr Elias M. Elias, Dept of Geology, University of Mosul for interesting discussions. The comments of Dr J. Omrani and an anonymous reviewer are acknowledged. Special thanks are due to the volume editor, Dr Olivier Lacombe, for his many constructive comments and suggestions. NA and HK acknowledge financial support from SIDA and VR.

References

AHMED, A. H., ARAI, S. & ATTIA, A. K. 2001. Petrological characteristics of podiform chromitites and associated peridotites of Pan African Proterozoic ophiolite complex of Egypt. *Mineralium Deposita* **36**, 72–84.

ALLAN, J. F., SACK, R. O. & BATIZA, R. 1988. Cr-rich spinels as petrogenetic indicators: MORB-type lavas from the Lamont seamount chain, eastern. *American Mineralogist* **73**, 741–53.

ALT, J. C. & SHANKS, W. C. 2003. Serpentinization of abyssal peridotites from the MARK area, Mid-Atlantic Ridge: sulfur geochemistry and reaction modelling. *Geochimica et Cosmochimica Acta* **67**, 641–53.

https://doi.org/10.1017/S0016756811000422 Published online by Cambridge University Press

ALVAREZ, W. 2010. Protracted continental collisions argue for continental plates driven by basal traction. *Earth and Planetary Science Letters* **296**, 434–42.

ARAI, S. 1992. Chemistry of chromian spinel in volcanic rocks as a potential guide to magma chemistry. *Mineralogical Magazine* **56**, 173–84.

ARAI, S. 1994. Compositional variation of olivine-chromian spinel in Mg-rich magma as guide of residual spinel peridotites. *Journal of Volcanology and Geothermal Research* **59**, 279–93.

ASWAD, K. J. 1999. Arc-continent collision in Northeastern Iraq as evidenced by Mawat and Penjwin Ophiolite Complexes. *Rafidain Journal of Science* **10**, 51–61.

ASWAD, K. J. & ELIAS, E. M. 1988. Petrogenesis, geochemistry and metamorphism of spilitized subvolcanic rocks of the Mawat Ophiolite Complex, NE Iraq. *Ofiolitti* **13**, 95–109.

AZIZ, N. R., ASWAD, K. J. & KOYI, H. A. 2011. Contrasting settings of serpentinite bodies in the northwestern Zagros Suture Zone, Kurdistan Region, Iraq. *Geological Magazine* **148**, 819–37. Published online 11 July 2011. doi:10.1017/S0016756811000409.

AZIZ, N. R., ELIAS, E. M. & ASWAD, K. J. 2011. Rb–Sr and Sm–Nd isotope study of serpentinites and their impact on the tectonic setting of Zagros Suture Zone, NE-Iraq. *Iraqi Bulletin of Geology and Mining* **7**, 67–75.

BABAEI, A., BABAIE, H. A. & ARVIN, M. 2005. Tectonic evolution of the Neyrez ophiolite, Iran: an accretionary prism model. *Ofioliti* **30**, 65–74.

BABAIE, H. A., BABAEI, A., GHAZI, A. M. & ARVIN, M. 2006. Geochemical, $^{40}Ar/^{39}Ar$ age and isotopic data for crustal rocks of the Neyriz ophiolite, Iran. *Canadian Journal of Earth Sciences* **43**, 57–70.

BABAIE, H. A., GHAZI, A. M., BABAEI, A., LA TOUR, T. E. & HASSANIPAK, A. A. 2001. Geochemistry of arc volcanic rocks of the Zagros crust zone, Neyriz, Iran. *Journal of Asian Earth Sciences* **19**, 61–76.

BARNES, S. J. & ROEDER, P. L. 2001. The range of spinel compositions in terrestrial mafic and ultramafic rocks. *Journal of Petrology* **42**, 2279–302.

BOILLOT, G., FERAUD, G., RECQ, M. & GIRARDEAU, J. 1989. Undercrusting by serpentinite beneath rifted margins. *Nature* **341**, 523–5.

BUDAY, T. 1980. *The Regional Geology of Iraq. Stratigraphy and Palaeogeography*. Baghdad: Publications of GEOSURV 1, 445 pp.

BUDAY, T. & JASSIM, S. Z. 1987. *The Regional Geology of Iraq. Tectonism, Magmatism and Metamorphism*. Baghdad: Publications of GEOSURV 1, 352 pp.

CANNAT, M., BIDEAU, D. & BOUGAULT, H. 1992. Serpentinized peridotites and gabbros in the Mid-Atlantic Ridge axial valley at 15°37′N and 16°52′N. *Earth and Planetary Science Letters* **109**, 87–106.

CANNAT, M., LAGABRIELLE, Y., BOUGAULT, H., CASEY, J., DE COUTURES, N., DMITRIEV, L. & FOUQUET, Y. 1997. Ultramafic and gabbroic exposures at the Mid-Atlantic Ridge: geological mapping in the 15 degrees N region. *Tectonophysics* **279**, 193–213.

COOKENBOO, H. O., BUSTIN, R. M. & WILKS, K. R. 1997. Detrital chromian spinel compositions used to reconstruct the tectonic setting of provenance implications for orogeny in the Canadian Cordillera. *Journal of Sedimentary Research* **67**, 116–23.

DHANNOUN, H. Y., AL-DABBAGH, S. M. A. & HASSO, A. 1988. The geochemistry of the Gercus Red Bed Formation of Northeast Iraq. *Chemical Geology* **69**, 87–93.

DICK, H. J. B. & BULLEN, T. 1984. Chromian spinel as a petrogenetic indicator in abyssal and alpine-type peridotites and spatially associated lavas. *Contributions to Mineralogy and Petrology* **86**, 54–76.

EVANS, B. W. & FROST, B. R. 1975. Chrome-spinel in progressive metamorphism – a preliminary analysis. *Geochimica et Cosmochimica Acta* **39**, 959–72.

FABRIÈS, J., BODINIER, J.-L., DUPUY, C., LORAND, J. P. & BENKERROU, C. 1989. Evidence for model metasomatism in the orogenic spinel lherzolite body from Caussou (Northeastern Pyrenees, France). *Journal of Petrology* **30**, 199–228.

FAKHARI, M. D., AXEN, G. J., HORTON, B. K., HASSANZADEH, J. & AMINI, A. 2008. Revised age of proximal deposits in the Zagros foreland basin and implications for Cenozoic evolution of the High Zagros. *Tectonophysics* **451**, 170–85.

FRYER, P. 1992. A synthesis of Leg 125 drilling of serpentine seamounts on the Mariana and Izu-Bonin forearcs. In *Proceedings of the Ocean Drilling Program Scientific Results, vol. 125* (eds P. Fryer, J. A. Pearce, L. D. Stocking, *et al.*), pp. 593–614. College Station, Texas.

GHARIB, F. & DE WEVER, P. 2010. Radiolaires mésozoïques de la formation de Kermanshah (Iran). *Comptes Rendus Palevol* **9**, 209–19.

HEBERT, R., HEKINIAN, R. & BIDEAU, D. 1997. Primitive intratransform volcanism at Garrett Transform Fault (East Pacific Rise). *Canadian Journal of Earth Sciences* **34**, 1101–17.

HORTON, B. K., HASSANZADEH, J., STOCKLI, D. F., AXEN, G. J., GILLIS, R. J., GUEST, B., AMINI, A., FAKHARI, M., ZAMANZADEH, S. M. & GROVE, M. 2008. Detrital zircon provenance of Neoproterozoic to Cenozoic deposits in Iran: implications for chronostratigraphy and collisional tectonics. *Tectonophysics* **451**, 97–122.

IRVINE, T. N. 1967. Chromian spinel as a petrogenetic indicator, Part II. Petrological applications. *Canadian Journal of Earth Sciences* **4**, 71–103.

JACKSON, E. D. 1969. Chemical variation in coexisting chromite and olivine in chromitite zones of the Stillwater Complex. *Economic Geology Monograph* **4**, 41–71.

JASSIM, S. Z. & BUDAY, T. 2006. Units of the unstable shelf and the Zagros Suture, Chapter 6. In *Geology of Iraq* (eds S. Z. Jassim & J. C. Goff), pp. 71–83. Brno, Czech Republic: Dolin, Prague and Moravian Museum.

JASSIM, S. Z., BUDAY, T., CICHA, I. & OPLETAL, M. 2006. Tectonostratigraphy of the Zagros Suture, Chapter 16. In *Geology of Iraq* (eds S. Z. Jassim & J. C. Goff), pp. 199–211. Brno, Czech Republic: Dolin, Prague and Moravian Museum.

KARIM, K. H., FATAH, A. I., IBRAHIM, A. O. & KOYI, H. A. 2009. Historical development of the present day lineaments of the western Zagros fold-thrust belts: a case study from Northeastern Iraq, Kurdistan Region. *Iraqi Journal of Earth Science* **9**, 55–70.

KOYI, H. A. 1988. Experimental modeling of the role of gravity and lateral shortening in the Zagros mountain belt. *American Association of Petroleum Geologists Bulletin* **72**, 1381–94.

LEE, Y. I. 1999. Geotectonic significant of detrital chromian spinel: a review. *Geosciences Journal* **3**, 23–9.

LEHMANN, J. 1983. Diffusion between olivine and spinel: application to geothermometry. *Earth and Planetary Science Letters* **64**, 123–38.

LINDQUIST, E. S. & GOODMAN, R. E. 1994. The strength and deformation properties of aphysical model mélange. In *Proceedings of the First North American Rock Mechanics Symposium (NARMS), Austin, Texas* (eds P. P.

Nelson & S. E. Laubach), pp. 843–50. Rotterdam: A.A. Balkema.

MICHAEL, P. J., LANGMUIR, C. H., DICK, J. B. H., SNOW, J. E., GOLDSTEIN, S. L., GRAHAM, D. W., LEHNERT, K., KURRAS, G., JOKAT, W., MUHE, R. & EDMONDA, H. N. 2003. Magmatic and amagmatic seafloor generation at the ultraslow-spreading Gakkel ridge, Arctic Ocean, *Nature* **423**, 956–61.

MOGHADAM, H. S., RAHGOSHAY, M. & FOROUZESH, V. 2009. Geochemical investigation of nodular chromites in the Forumad ophiolite, NE Iran. *Iranian Journal of Science & Technology Transaction A*. **33**(A1), 103–8.

MOGHADAM, H. S. & STERN, R. J. 2010. Late Cretaceous forearc ophiolites of Iran. *Island Arc* **20**, 1–4.

NICOLAS, A. 1985. Novel type of crust produced during continental rifting. *Nature* **315**, 112–15.

OMRANI, J., AGARD, P., WHITECHURCH, H., BENOIT, M., PROUTEAU, G. & JOLIVET, L. 2008. Arc-magmatism and subduction history beneath the Zagros Mountains, Iran: a new report of adakites and geodynamic consequences. *Lithos* **106**, 380–98.

O'NEILL, H. S. T. C. 1981. The transition between spinel lherzolite and garnet lherzolite and its use as a geobarometer. *Contributions to Mineralogy and Petrology* **77**, 185–94.

O'NEILL, H. S. T. C. & WOOD, B. J. 1979. An experimental study of partitioning between garnet and olivine and its calibration as a geothermometer. *Contributions to Mineralogy and Petrology* **70**, 59–70.

PARKINSON, I. J. & PEARCE, J. A. 1998. Peridotites from the Izu-Bonin-Mariana forarc (ODP Leg 125): evidence for mantle melting and melt-mantle interaction in a suprasubduction zone setting. *Journal of Petrology* **39**, 1577–618.

POBER, E & FAUPL, P. 1988. The chemistry of detrital chromian spinels and its implications for the geodynamic evolution of the eastern Alps. *Geologische Rundschau* **77**, 641–67.

PROENZA, J. A., ORTEGA-GUTIERREZ, F., CAMPRUBI, A., TRITLLA, J., ELIAS-HERRERA, M. & REYES-SALAS, M. 2004. Paleozoic serpentinite-enclosed chromitites from Tehuitzingo (Acatlan Complex, southern Mexico): a petrological and mineralogical study.*Journal of South American Earth Sciences* **16**, 649–66.

QUICK, J. E. & GREGORY, R. T. 1995. Significance of melt-wall rock reaction: a comparative anatomy of three ophiolites. *Journal of Geology* **103**, 187–98.

ROEDER, P. L. 1994. Chromite from the fiery rain of chondrules to Kilauea lava lake. *The Canadian Mineralogist* **32**, 729–46.

ROEDER, P. L., CAMPBELL, I. H. & JAMIESON, H. E. 1979. A re-evaluation of the olivine-spinel geothermometer. *Contributions to Mineralogy and Petrology* **68**, 325–34.

SACK, R. O. & GHIORSO, M. S. 1991. Chromian spinel as petrogenetic indicators: thermodynamics and petrological applications. *American Mineralogist* **76**, 827–47.

TAKAHASHI, N. & ARAI, S. 1989. Textural and chemical features of chromian spinel–pyroxene symplectites in the Horoman peridotites, Hokkaido, Japan. *Science Reports of the Institute of Geoscience, University of Tsukuba, Section B* **10**, 45–55.

STEVENS, R. E. 1944. Composition of some chromites of the western hemisphere. *American Mineralogist* **29**, 1–34.

WHITMARSH, R. B., MANATSCHAL, G. & MINSHULL, T. A. 2001. Evolution of magma-poor continental margins from rifting to seafloor spreading. *Nature* **413**, 150–4.